Multiplex detection of collisional energy transfer using KCSFI†

Heiko Frerichs,[a] Thomas Lenzer,*[ab] Klaus Luther[a] and Dirk Schwarzer[b]

[a] Institut für Physikalische Chemie, Universität Göttingen, Tammannstr. 6, D-37077 Göttingen, Germany. Fax: +49 551 39 3150; Tel: +49 551 39 12598
[b] Max-Planck-Institut für biophysikalische Chemie, Abteilung 010, Am Fassberg 11, D-37077 Göttingen, Germany. E-mail: tlenzer@gwdg.de; Fax: +49 551 201 1501; Tel: +49 551 201 1344

A new detection method for obtaining collisional transition probabilities $P(E',E)$ of highly vibrationally excited molecules in the gas phase is presented. The technique employs energy-selective probing of the time-dependent vibrational population distribution by "kinetically controlled selective *fluorescence* (KCSF)". We present experimental results for a test system, the collisional deactivation of toluene by argon, where we use the well-known "kinetically controlled selective *ionization* (KCSI)" scheme as a reference for comparison. A newly designed setup is employed that allows simultaneous detection of fluorescence and ionization signals under identical experimental conditions ("kinetically controlled selective fluorescence and ionization = KCSFI"). For the system toluene + argon it is demonstrated that KCSF and KCSI yield identical results. A rate-equation model is presented to understand common features and differences of both approaches. The fluorescence detection scheme shows promise for future investigations on collisional energy transfer. The experimental setup is simpler, because it requires no additional ionization wavelength. This will hopefully give access to the $P(E',E)$ of systems where, *e.g.*, ionization schemes are difficult to implement due to short wavelengths required for the ionization step. A few examples will be outlined briefly.

1. Introduction

Direct experimental techniques to study collisional energy transfer (CET) of highly vibrationally excited molecules are of central importance to characterize the energy dependent efficiency of collisions and understand the mechanisms of CET.[1,2] Early methods like "infrared fluorescence (IRF)"[3,4] or "ultraviolet absorption (UVA)"[5,6] have provided quantities averaged over the whole population distribution during deactivation, mainly the first moment of energy transfer $\langle \Delta E \rangle$ and its energy dependence. With the advent of the method of "kinetically controlled selective ionization (KCSI)" it has finally become possible to measure complete distributions of the central quantity of collisional energy transfer, the collisional transition probability $P(E',E)$, over wide ranges of vibrational energy and also to improve the accuracy of energy dependent CET parameters like $\langle \Delta E \rangle$ by up to one order of magnitude.[7–9] $P(E',E)$ characterizes the energy transfer behavior in a system completely, and is needed as input, *e.g.*, in master equation simulations for combustion models. In this paper we present an alternative approach for detection named "kinetically controlled selective fluorescence (KCSF)". This technique not only provides an equivalent information content on CET, but also opens up new perspectives to investigate systems in which the two-photon ionization technique of KCSI experiences technical problems.
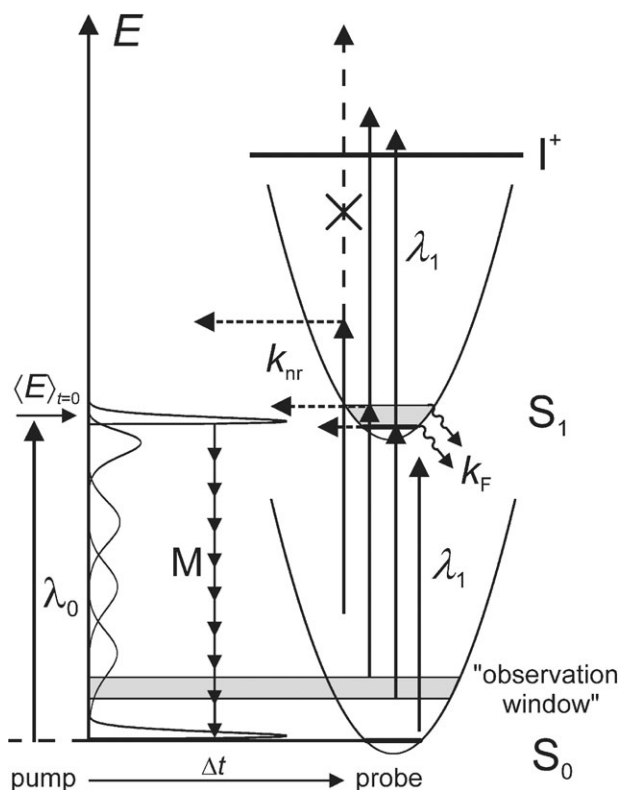
A basic scheme of the KCSF and KCSI pump–probe experiments for toluene is shown in Fig. 1. Briefly, at $t = 0$ a quasi-microcanonical population of highly vibrationally excited molecules is prepared in the ground electronic state (S_0^*) by a pump laser (wavelength λ_0). After preparation, the S_0^* molecules are deactivated in a collision cascade with a low

pressure (mbar range) bath gas M and finally reach thermal equilibrium. This is shown on the left side of Fig. 1 by a sequence of schematic population distributions. They relax and broaden in S_0 during the sequence of collisions with M, before they finally return back into the ambient temperature Boltzmann distribution.

In the KCSI process the S_0^* molecules are detected by a pulsed laser resonant two-photon ionization process after a time delay Δt. This is shown on the right side of the figure. By absorption of a photon with the wavelength λ_1 the molecules in S_0^* are pumped into an intermediate electronic state (*e.g.*, S_1). A kinetic competition between ionization with a second photon of wavelength λ_1 [rate coefficient $k_2(E)$] and depletion of the intermediate state population due to nonradiative processes and fluorescence with a total rate coefficient $k_{tot}(E) = k_{nr}(E) + k_F(E)$ takes place. The states reached by depopulation of S_1 cannot be further ionized at λ_1. The ionization is therefore *kinetically controlled* by the ratio of $k_2(E)$ and $k_{tot}(E)$. The strong increase of $k_{tot}(E)$ with S_1 excess energy allows the *selection* of a narrow energy range for the resonant two-step *ionization* in the S_1 state (upper grey stripe in Fig. 1). This energy band is projected down onto the S_0 manifold by the photon energy at λ_1: As a result an energetic "observation window" $W_{KCSI}(E,\lambda_1)$ is formed, as indicated by the lower grey stripe in Fig. 1. The lower energy edge of this window is defined by the constraint of the minimum vibrational energy necessary to reach the S_1 origin with a λ_1 photon. The observation window is shifted by tuning λ_1. Therefore the relaxing population distribution can be monitored at different positions on the S_0 energy scale.

For KCSF the population evolution in the relevant energy range (window) of the S_0 state during time dependent probing of the relaxation is no longer oberved *via* an additional ionization step. Instead, the fluorescence from the intermediate state S_1 is detected (Fig. 1). The yield of these fluorescence

† Dedicated to Prof. Dr Michael Buback on the occasion of his 60th birthday.

Fig. 1 Simplified KCSFI scheme for toluene. The relaxing distribution of highly vibrationally excited S_0^* molecules is monitored through a narrow "observation window" by collecting either fluorescence photons from the S_1 state (KCSF) or by detecting ions from a resonant two-photon process *via* the S_1 state (KCSI).

photons is also kinetically controlled, and determined by the energy dependent ratio of the fluorescence rate constant $k_F(E)$ and the total depopulation rate constant $k_{tot}(E)$, *i.e.*, the energy dependent fluorescence quantum yield $\Phi_F(E)$ in the S_1 state. This gives rise to a KCSF "observation window" $W_{KCSF}(E,\lambda_1)$, which not necessarily has the same shape as the KCSI window function $W_{KCSI}(E,\lambda_1)$. A more detailed discussion of the KCSF and KCSI windows on basis of a rate-equation approach will be presented in Section 3.2. The time-dependent KCSF and KCSI signals $I_F(t)$ and $I_D(t)$ are described as a convolution of the respective window function and the time-dependent vibrational distribution $g(E,t)$ in the S_0 state:

$$I_F(t) \propto \int_0^\infty g(E,t)W_{KCSF}(E,\lambda_1)dE \qquad (1)$$

$$I_D(t) \propto \int_0^\infty g(E,t)W_{KCSI}(E,\lambda_1)dE \qquad (2)$$

Time-resolved fluorescence yields from an electronically excited state in a pump–probe experiment have been reported earlier on, in order to deduce from it vibrational temperatures of ground state *trans*-stilbene in liquids.[10,11] Subsequently, Nikowa *et al.* started attempts to implement the fluorescence analogue of KCSI for the collisional deactivation of *trans*-stilbene in liquid *n*-pentane and methanol, and KCSI type signals could be observed.[12] However, even then the interpretation of these experiments was not straightforward. Obviously, the signals obtained in the condensed phase not only probe the deactivation in the ground electronic state but are also influenced by collisional deactivation in the electronically excited state, due to the very high collision rate under these conditions which can efficiently compete with the S_1 fluorescence rate. Moreover a 352 nm interference filter (bandwidth 22 nm) was used, so that a slice of the integral fluorescence was detected. The resulting influence on the shape of the window function $W_{KCSF}(E,\lambda_1)$ remained still unclear. Consequently, the extraction of well-defined energy transfer properties in the

ground electronic state was not possible. The different situation in the condensed phase is also confirmed by very recent measurements for *trans*-stilbene under gas phase conditions, where deactivation in the S_1 state can be safely ruled out. Experiments using KCSI and KCSF detection[13–15] show shapes of relaxation signals and dependences on the probe wavelength that differ from the results in the liquid phase.

Obviously, a direct experimental comparison of the two methods is necessary to evaluate the performance and differences of the KCSF detection scheme relative to the well-established KCSI process under identical conditions. For this reason we have constructed a new cell allowing the simultaneous detection of KCSF and KCSI signals (KCSFI). We report here our first results with this setup obtained for the collisional deactivation of highly vibrationally excited toluene ("toluene*") in an argon bath. Interestingly, we find that at our conditions KCSF and KCSI time-dependent signals show practically the same shape. We will interpret both signals in terms of a master equation approach, in which the contributions of different photophysical parameters to the shape of the KCSF and KCSI observation windows will be analyzed by a rate equation model of the competitive processes.
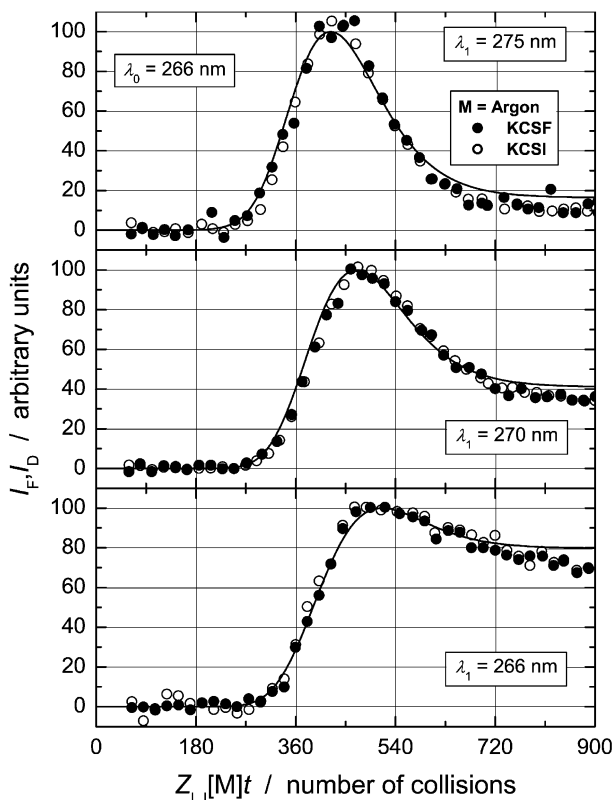
2. Experimental technique

The KCSI experiment has been described in detail in our earlier publications,[8,9] so we focus here only on some specifics of the fluorescence setup. Briefly, the detection flow cell has four ports, two of them carrying window mounts at Brewster's angles each equipped with Suprasil I windows allowing passage of the laser beams into the cell. One port at 90° with respect to the laser beams features an additional Suprasil I window, through which the fluorescence is monitored by an integrating UV-sensitive photomultiplier (Hamamatsu 1P28A). Efficient reduction of stray light is achieved by Wood's horns (minimizing back reflections from the windows inside the cell) and by two sets of laser baffles. This arrangement allows collection of integral fluorescence signals without the need of using filters for suppressing the laser background signal. This has the additional advantage that one minimizes possible distortions of the KCSF signal, which is emitted in the same wavelength region. Only a single UG11 filter (Schott) was used to prevent visible stray light from entering the detector. This bandpass filter is very well suited for detecting the emission from hot and cold toluene molecules, which occurs in the wavelength range between 260 nm and 380 nm.[16,17] In addition to the fluorescence setup, a sensitive capacitor arrangement was installed inside the cell as described in our earlier KCSI publications,[8] with a lower detection limit of a few hundred ions.

Highly vibrationally excited toluene molecules ("toluene*") were prepared *via* excitation of the isomeric precursor 1,3,5-cycloheptatriene at $\lambda_0 = 266$ nm using a frequency-quadrupled Nd:YAG laser (Continuum Surelite-I). Detection wavelengths $\lambda_1 = 266$–275 nm were generated by a frequency-doubled excimer pumped dye laser (Lambda Physik LPX 105i and LPD 3002). KCSF and KCSI curves were simultaneously detected in a counterpropagating beam-in-beam arrangement by scanning the delay time between the pump and probe pulses. The ion and fluorescence signals were extracted using series of carefully controlled difference measurements in a fashion very similar to that described previously.[8]

3. Results and discussion

3.1. Comparison and modeling of KCSF and KCSI curves

Fig. 2 shows the results for the collisional deactivation of highly vibrationally excited toluene with an initial average energy of 49 380 cm^{-1} in 25.5 mbar argon at three different probe wavelengths λ_1. The time axis has been normalized to a "number of collisions" scale using the Lennard-Jones collision

Fig. 2 Comparison of KCSF (●) and KCSI (○) signals for the collisional deactivation of toluene* by argon (P_{tot} = 25.5 mbar) for three different observation windows (λ_1 = 275, 270 and 266 nm). Excitation of the isomeric precursor CHT at λ_0 = 266 nm. Solid lines: Master equation simulations using a monoexponential $P(E',E)$ with parametric exponent Y in the argument [eqn. (3)]. The best fit parameters from ref. 9 were employed (C_0 = 43.5 cm^{-1}, C_1 = 4.20 × 10^{-3}, Y = 0.7). Note the identical position and shape of the KCSF and KCSI signals.

number 1.088 × 10^7 mbar^{-1} s^{-1}.[8] Interestingly the KCSF and KCSI signals are practically indistinguishable within the accuracy of the experiment, and this is also observed in additional experiments at much lower pressures (2.8 mbar). This result is not necessarily expected *a priori* (see below). The KCSF signals show the same typical dependence on λ_1 as known from KCSI curves: The fluorescence observation window at the longest wavelength (275 nm) is highest up on the energy scale, so the KCSF signal appears earliest. The residual fluorescence is due to the overlap of the KCSF observation window with the thermal toluene Boltzmann distribution. With decreasing wavelength, the windows are shifted down the energy scale so the initial rise of the corresponding KCSF signals appears at increasingly later times. In addition, the level of the fluorescence signal after complete deactivation at the end of our measurements increases, because these windows have an increasingly larger overlap with the vibrational Boltzmann distribution of relaxed toluene at the room temperature of the experiment.

Also included in Fig. 2 are master equation simulations (solid lines) using our well-proven empirical minimum parameter expression of the transition probability $P(E',E)$ for downward collisions (upward collisions defined by detailed balance):[7,9]

$$P(E',E) = \frac{1}{c(E)}\exp\left[-\left(\frac{E-E'}{\alpha(E)}\right)^Y\right]$$

$$= \frac{1}{c(E)}\exp\left[-\left(\frac{E-E'}{C_0+C_1E}\right)^Y\right], (E' \leq E) \quad (3)$$

$P(E',E)$ is monoexponential with an energy dependent parameter $\alpha(E) = C_0 + C_1E$ and a parametric exponent Y in the argument. Y determines the shape of the decay. $\alpha(E)$ describes the width of the CET probability and is therefore directly related to the efficiency of the collisions. $c(E)$ is a normalization constant. In all cases of relaxations from very high levels of vibrational excitation in various bath gases studied so far, the experimental KCSI signals could consistently be modeled with this functional form. For toluene*, the exponents Y vary smoothly with the "size" of the collider, with values between Y = 0.65 (toluene* + helium) and 1.5 (toluene* + *n*-heptane). The linear dependence of the width parameter α on energy leads to an approximately linear energy dependence of the first moment of energy transfer $\langle\Delta E\rangle$, the average energy transferred per collision, and the square root of the second moment of energy transfer $\langle\Delta E^2\rangle^{1/2}$, where the moments $\langle\Delta E^n\rangle$ are defined as:

$$\langle\Delta E(E)^n\rangle = \int_0^\infty (E'-E)^n P(E',E)\mathrm{d}E' \quad (4)$$

As one can see in Fig. 2 both the KCSF and KCSI data are well described by our optimized parameters from earlier experiments (C_0 = 43.5 cm^{-1}, C_1 = 4.20 × 10^{-3}, Y = 0.7).[9] KCSI window functions as already presented in our earlier publication were used for modeling. A more detailed discussion of the KCSF and KCSI observation windows can be found in the following sections.

3.2. Rate-equation model for KCSI and KCSF processes

To understand the relation between a KCSI signal (ion yield produced by a two-photon ionization *via* a resonant intermediate state) and a KCSF curve (fluorescence from the resonant intermediate state after one-photon absorption) it is important to compare expressions for the yield of KCSI ions and KCSF fluorescence photons. Because no coherent population-transfer, like *e.g.*, Rabi cycling, occurs under our experimental conditions (weak field limit) a rate-equation approach is adequate. Such descriptions have been frequently applied in the literature to describe *inter alia* multiphoton and fluorescence processes involving multiple levels.[18–22] Here, we outline and extend an approach by Bischel and co-workers.[18] A four-level model can be used to describe the toluene system (see also Fig. 1), and the following rate-equations can be set up. Note that in eqn. (5) a misprint in Bischel's original paper is corrected by removing a factor of 2:

$$\frac{\mathrm{d}S_1}{\mathrm{d}t} = \frac{I(t)}{h\nu}[\sigma_{10}S_0 - (\sigma_{01} + \sigma_{21})S_1] - k_{tot}S_1 \quad (5)$$

$$\frac{\mathrm{d}I^+}{\mathrm{d}t} = \frac{I(t)}{h\nu}\sigma_{21}S_1 \quad (6)$$

$$\frac{\mathrm{d}F}{\mathrm{d}t} = k_F S_1 \quad (7)$$

S_0, S_1 and I^+ are the toluene populations in a specific vibrational level of the ground electronic state, the first electronically excited state and the ion state, respectively. Toluene molecules can disappear from the vibrational level of the S_1 state by nonradiative transitions with the rate constant k_{nr}. They are also removed by radiative processes with the rate constant k_r. For our case of S_1 toluene, only fluorescence is relevant, so that $k_r = k_F$. Consequently, F in eqn. (7) represents the number of photons emitted by toluene molecules which disappear from the vibrational level of the S_1 state by fluorescence with the rate constant k_F. The total depopulation rate constant for the level in S_1 is then $k_{tot} = k_F + k_{nr}$. All molecules following the radiative and nonradiative channels are lost for the ionization process. σ_{10} and σ_{21} are the absorption cross sections from the ground electronic state ($S_1 \leftarrow S_0$) and the first

electronically excited state ($I^+ \leftarrow S_1$), respectively. σ_{01} is the cross section for stimulated emission from the S_1 down to the S_0 state. $I(t)$ and ν represent the laser intensity and frequency, respectively.

For small laser intensities two approximations can be made which are fulfilled under our conditions. Firstly, depopulation of the S_1 level due to stimulated emission and ionization is negligible, so the second term in the squared brackets in eqn. (5) can be removed. Secondly, the S_0 state is, in practical terms, not depleted [$S_0(t) \approx S_0(t = 0) = $ constant].[18] Then eqn. (5) transforms into:

$$\frac{dS_1}{dt} + k_{tot}S_1 = \frac{I(t)}{h\nu}\sigma_{10}S_0 \qquad (8)$$

After introducing the normalized laser intensity $\chi(t) = I(t) A/E$ (E = laser pulse energy, A = cross section of the laser beam) one obtains:

$$S_1 = \frac{E\sigma_{10}S_0}{Ah\nu}\exp(-k_{tot}t)\int_{-\infty}^{t}\chi(t')\exp(k_{tot}t')dt' \qquad (9)$$

For the KCSI process we need to know the ion yield I^+. Insertion into eqn. (6) and integration yields:

$$I^+ = \left(\frac{E}{Ah\nu}\right)^2 S_0\sigma_{10}\sigma_{21}\int_{-\infty}^{+\infty}\chi(t)\exp(-k_{tot}t)$$
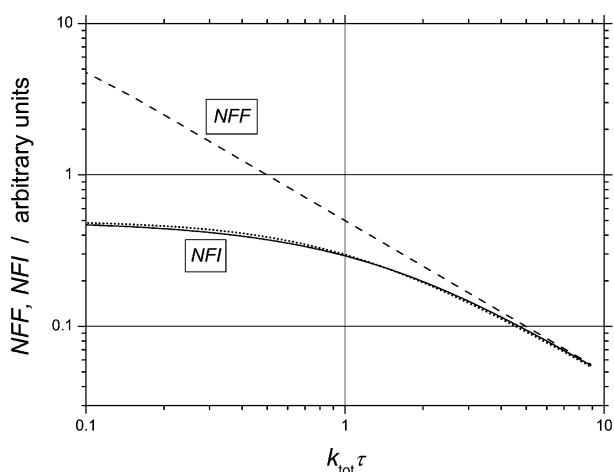$$\times \left(\int_{-\infty}^{t}\chi(t')\exp(k_{tot}t')dt'\right)dt \qquad (10)$$

One can define the "normalized fractional ionization (NFI)" as:[18]

$$\text{NFI} = \int_{-\infty}^{+\infty}\chi(t)\exp(k_{tot}t)(\int_{-\infty}^{t}\chi(t')\exp(k_{tot}t')dt')dt \qquad (11)$$

In a KCSI experiment one typically uses a laser with a pulse length t_{FWHM} of about 10 ns. If we assume a Gaussian shape for the laser intensity it is possible to calculate the NFI numerically as a function of the product $k_{tot}\tau$ (for a Gaussian pulse $\tau = 0.753t_{FWHM}$). The result is shown in Fig. 3 in a double-logarithmic fashion (solid line). Two limiting cases can be distinguished for the NFI. For $k_{tot}\tau \ll 1$ eqn. (11) simplifies to:

$$\text{NFI} = \int_{-\infty}^{+\infty}\chi(t)(\int_{-\infty}^{t}\chi(t')dt')dt = 0.5 \qquad (12)$$

i.e., the NFI reaches a *constant* value of 0.5 for arbitrary normalized laser pulses. For the other limit ($k_{tot}\tau \gg 1$)

Fig. 3 Comparison of the normalized fractional fluorescence (NFF) and normalized fractional ionization (NFI) for KCSF and KCSI experiments, respectively. Solid line: NFI calculated *via* eqn. (11) for a Gaussian laser pulse with $t_{FWHM} = 10$ ns ($\tau = 7.53$ ns). Dotted line: Approximation of the NFI as given in eqn. (14). Dashed line: NFF from eqn. (20), rescaled by a constant factor to demonstrate the same asymptotic behavior of NFI and NFF for large values of $k_{tot}\tau$.

one finds:

$$\text{NFI} = \frac{1}{k_{tot}}\int_{-\infty}^{+\infty}\chi^2(t)dt \qquad (13)$$

In this case the NFI is proportional to the inverse of the total depopulation rate constant k_{tot} in the intermediate state S_1. Both limiting cases are clearly visible in Fig. 3. An analytical expression for calculating the KCSI observation windows has proved itself to be very useful in approximating the NFI. It works very well, even for the non-Gaussian pulse shapes of, e.g., typical ns Nd:YAG lasers:[18]

$$\text{NFI} \approx 0.5[1 + (k_{tot}\tau)^{4/3}]^{-3/4} \qquad (14)$$

This curve is also included in Fig. 3 as a dotted line. Combining eqns. (10) and (14) yields:

$$I^+ \propto \sigma_{10}\sigma_{21}[1 + (k_{tot}\tau)^{4/3}]^{-3/4} \qquad (15)$$

Summing up over the full quasicontinuum of vibrational levels, and changing to integration over E, one obtains the well-known KCSI window function W_{KCSI}, as used in the interpretation of our earlier experiments, given here for the case of the one-color two-photon ionization of toluene:[7–9,23]

$$W_{KCSI}(E(S_0^*),\lambda_1) \propto \sigma_{10}(\lambda_1,E(S_0^*))\, \sigma_{21}(\lambda_1,E(S_1^*))$$
$$\times [1 + (k_{tot}(E(S_1^*))\tau)^{4/3}]^{-3/4} \text{ for } E \geq E_{low} \qquad (16)$$

$$W_{KCSI}(E(S_0^*),\lambda_1) = 0 \text{ for } E < E_{low} \qquad (17)$$

E_{low} is the minimum energy in S_0 at which two-photon ionization becomes possible, i.e., $E_{low} = E_{0-0}(S_1)$-hc/λ_1, where E_{0-0} (S_1) is the 0–0 transition energy of toluene (37 485 cm^{-1}).[24]

In the following we turn to the KCSF process. The number of fluorescence photons F emitted from an intermediate state level was already given in eqn. (7). Combination with eqn. (9) and subsequent integration yields:

$$F = \frac{ES_0}{Ah\nu}\sigma_{10}k_F\int_{-\infty}^{+\infty}\exp(-k_{tot}t)\left(\int_{-\infty}^{t}\chi(t')\exp(k_{tot}t')dt'\right)dt \qquad (18)$$

In analogy to the KCSI process one can define a "normalized fractional fluorescence (NFF)" as:

$$\text{NFF} = \int_{-\infty}^{+\infty}\exp(-k_{tot}t)(\int_{-\infty}^{t}\chi(t')\exp(k_{tot}t')dt')dt \qquad (19)$$

For arbitrary values of $k_{tot}\tau$ the NFF is given by:

$$\text{NFF} = \frac{1}{k_{tot}} \qquad (20)$$

i.e., it is proportional to the inverse of the total depopulation rate constant k_{tot}. For comparison we have included the NFF curve in Fig. 3 as a dashed line. If $k_{tot}\tau$ is large, both the NFI and NFF show the same dependence ($\propto k_{tot}^{-1}$). However, at low $k_{tot}\tau$, the NFI levels off. This is due to the fact, that in the ionization case the S_1 population is only probed within the "gate time" (laser pulse width) of the ionization step, whereas fluorescence photons are emitted as long as there is a S_1 population. In the limiting case of very large $k_{tot}\tau$, the population decay in S_1 happens on a time scale much shorter than the laser pulse length, so practically no fluorescence is emitted after the laser is off, leading to the same k_{tot}^{-1} dependence of the NFI and NFF.

Substituting eqn. (20) into eqn. (18) yields:

$$F = \frac{ES_0}{Ah\nu}\sigma_{10}\frac{k_F}{k_{tot}} = \frac{ES_0}{Ah\nu}\sigma_{10}\Phi_F \propto \sigma_{10}\Phi_F \qquad (21)$$

i.e., the number of fluorescence photons is proportional to the absorption cross section σ_{10} in S_0 and the fluorescence quantum yield $\Phi_F = k_F/k_{tot}$ in the S_1 state. Note that this equation is the KCSF counterpart of eqn. (15). The corresponding window

function W_{KCSF} is immediately obtained as:

$$W_{KCSF}(E(S_0^*),\lambda_1) \propto \sigma_{10}(\lambda_1,E(S_0^*))\,\Phi_F(E(S_1^*))\text{ for}$$
$$E \geq E_{low} \qquad (22)$$

$$W_{KCSF}(E(S_0^*),\lambda_1) = 0 \text{ for } E < E_{low} \qquad (23)$$

Finally we compare the relative yields of the KCSI and KCSF processes. We combine eqns. (10) and (18) to obtain the ratio of the number of ions and fluorescence photons. If both signals are detected under identical conditions (laser energies and beam diameters) one obtains:

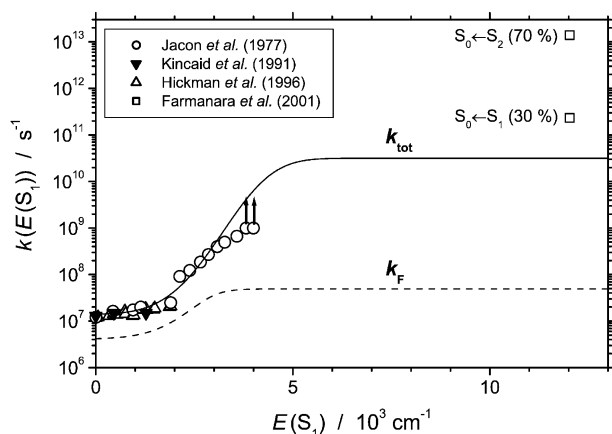$$\frac{I^+}{F} \propto \frac{\sigma_{21}}{k_F}\frac{NFI}{NFF} \qquad (24)$$

For the special case of large $k_{tot}\tau$ it has already been mentioned that the NFI and NFF show the same k_{tot}^{-1} dependence. eqn. (24) then reads:

$$\frac{I^+}{F} \propto \frac{\sigma_{21}}{k_F} \qquad (25)$$

If the absorption cross section σ_{21} for the second step in the KCSI process and the fluorescence rate constant k_F of the KCSF process are both *energy independent* or show the *same type of energy dependence* then the KCSI and KCSF window functions will have an identical shape. In these cases, KCSI and KCSF signals should look exactly the same.

3.3. Application to toluene

The assumption of a constant σ_{21} probably holds sufficiently well for toluene and other aromatics in the wavelength range of practical interest, as discussed earlier.[7,9,25] The question, to which regime of $k_{tot}\tau$ in Fig. 3 the NFI and NFF belong in the case of toluene, is answered by inspection of the energy dependence of k_{tot}. In Fig. 4 a plot of k_{tot} is shown as a function of S_1 excess energy. The points represent time-resolved measurements from four different sources.[24,26–28] The solid line is our earlier fit to these data,[9] at the time where the measurements from Farmanara et al.[28] were not yet available. These authors conclude, that 70% of the toluene molecules with about 12 000 cm^{-1} excess energy (S_2 excitation) take a direct internal conversion (IC) pathway $S_0 \leftarrow S_2$ with a rate constant $k_{02} = 1.4 \times 10^{13}$ s^{-1}, 30% of the molecules relax *via* a stepwise IC mechanism $S_0 \leftarrow S_1 \leftarrow S_2$ with $k_{01} = 2.3 \times 10^{11}$ s^{-1} for the second step. These newer experimental values are more

than one order of magnitude higher than in our more conservative earlier extrapolation based on the behavior of the related benzene molecule.[9] It is a nice side effect, that the new data definitely prove that the KCSI (and KCSF) window functions will not "open up" again at high energies, due to the influence of the increase of σ_{10} with energy. This was already ruled out indirectly in our earlier paper on the basis of the observed KCSI signal shape. For the following discussion we therefore keep our original function for $k_{tot}(E)$, which is sufficiently accurate for energies up to 10 000 cm^{-1}. Future fits should consider the new data at 12 000 cm^{-1} and will hopefully be based on additional experiments filling up the gap at intermediate S_1 excess energies. Taking the values from our fit, $k_{tot}(E)$ varies between 1.4×10^7 and 3.2×10^{10} s^{-1}. For $\tau = 7.53$ ns (Gaussian laser pulse with 10 ns FWHM) this corresponds to $k_{tot}\tau$ values between 0.11 and 238. This means that at low S_1 excess energies the k_{tot} dependence of the NFI and NFF will be different (Fig. 3).

We will now consider the influence of energy dependence of the fluorescence rate constant k_F. This is done by using fluorescence quantum yield measurements by Noyes and coworkers,[16,24] plotted in Fig. 5 as open circles. For comparison, we first calculate a hypothetical Φ_F curve for an energy independent $k_F = 4.1 \times 10^6$ s^{-1} (solid line). This value is extracted from our fit in Fig. 4 ($k_{tot} = 1.4 \times 10^7$ s^{-1} at the S_1 origin) and an estimate for the fluorescence quantum yield $\Phi_F = 0.29$, from ref. 16 mentioned above. As one can see, an energy independent k_F is not consistent with the experimental data in Fig. 5. Introducing energy dependence for the fluorescence rate constant we obtain good agreement with the experimental points by using an energy dependent scaling function $S(E)$, so that $k_F(E) = S(E)4.1 \times 10^6$ s^{-1}, where E is the excess energy in S_1:

$$S(E) = \exp[d + a(E/\text{cm}^{-1} - c) - (\{a\text{ abs}(E/\text{cm}^{-1} - c)\}^e$$
$$+ b^e)^{(1/e)}] + f \qquad (26)$$

The resulting fit in Fig. 5 (dashed line) is obtained for the parameter set $a = 0.001\,94$, $b = 13.600\,68$, $c = -4002.357\,66$, $d = 2.401\,51$, $e = 27.456\,14$ and, $f = 0.986\,08$. The corresponding energy dependent $k_F(E)$, which represents the correct $\Phi_F(E)$, is plotted as a dashed line in Fig. 4.

We are now in the position to calculate the KCSF window functions *via* eqns. (22) and (23) and compare them with their KCSI counterparts [eqns. (16) and (17)].[9] An example is shown in Fig. 6 for $\lambda_1 = 275$ nm. Both have been normalized to a maximum amplitude of 100. Only small differences between the KCSF window (dashed line) and the KCSI window (solid line)

Fig. 4 Energy dependence of the rate constant $k(E)$ for toluene in the S_1 state. Time-resolved measurements of $k_{tot}(E)$ from refs. 24, 26, 27 and 28. Solid line: fit from ref. 9, dashed line: estimated fluorescence rate constant $k_F(E)$ which reproduces the experimental fluorescence quantum yields $\Phi_F(E)$ shown in Fig. 5.[16,24] The experiments of Jacon et al. ($\bigcirc$) have a time resolution of about 1 ns, so their two points at the highest energies are probably lower limits to the true value, as indicated by the two arrows.[24]
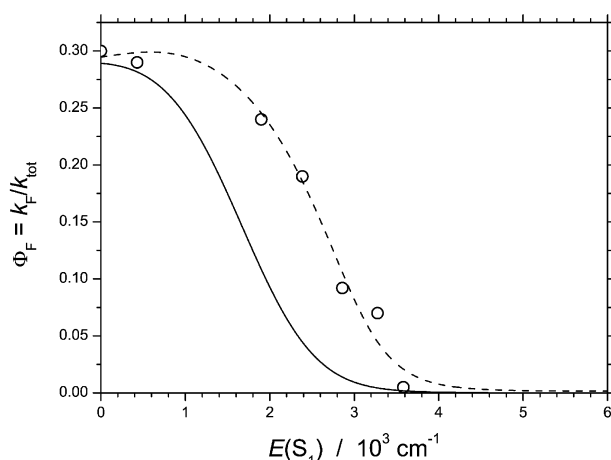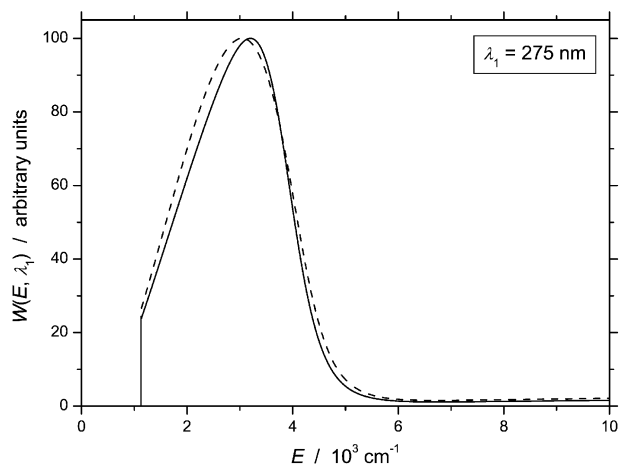

Fig. 5 Energy dependence of the fluorescence quantum yield $\Phi_F(E)$ for toluene in the S_1 state. $\bigcirc$: Data from Burton et al.,[16,24] solid line: calculated on the basis of $k_{tot}(E)$ from Fig. 4 and an energy independent $k_F = 4.1 \times 10^6$ s^{-1}, dashed line: same as the solid line, but using the energy dependent $k_F(E)$ from Fig. 4.

Fig. 6 Comparison of KCSF and KCSI observation windows for toluene at the probe wavelength $\lambda_1 = 275$ nm. Solid line: KCSI window function,[9] dashed line: KCSF window with energy dependent k_F from Fig. 4. Note the similarity of both window shapes.

can be seen. An analogous behavior is found for the observation windows at the other probe wavelengths. Considering the fact that there are definitely certain error limits of the fluorescence quantum yields $\Phi(E)$ (which are however difficult to quantify at present) it is safe to say that the KCSF and KCSI windows for toluene have essentially the same shape. This result is consistent with the experimental findings in Fig. 2, which show that the KCSF and KCSI signals at the three probe wavelengths λ_1 are virtually indistinguishable. We also note at this point that the master equation simulations are rather robust against changes in the detailed shape of the window functions, as was already discussed in detail earlier.[9]

4. Conclusions

We have presented experimental results of a new technique, "kinetically controlled selective *fluorescence* (KCSF)", for obtaining $P(E',E)$ distributions characterizing CET of highly vibrationally excited molecules. The deactivation of toluene in an argon bath was studied as a test system, and referenced against data from the well-known "kinetically controlled selective *ionization* (KCSI)" scheme. This accurate comparison became possible using a newly designed setup, which allows *simultaneous detection of fluorescence and ionization* signals under identical experimental conditions ("kinetically controlled selective fluorescence and ionization = KCSFI"). The curves for toluene* + Ar have a virtually indistinguishable shape. The experimental results can be interpreted in the framework of a rate-equation approach. It was found that with typical nanosecond laser pulses ($t_{FWHM} \approx 10$ ns) and high depopulation rates in the S_1 state (k_{tot} larger than roughly 3×10^8 s^{-1}) the yield of ions and fluorescence photons are both proportional to k_{tot}^{-1}, the inverse of the depopulation rate constant in the intermediate state. If the absorption cross section for the second photon in the KCSI process and the fluorescence rate constant in the KCSF process are energy independent (or in the same way energy dependent) KCSF and KCSI signals will have *exactly the same shape*. In the toluene case however, k_{tot} is fairly small at low S_1 excess energies. The agreement of the KCSI and KCSF signals can then however easily be rationalized by the energy dependence of the fluorescence rate constant k_F which follows from literature fluorescence quantum yields Φ_F. Note also that collisions, which happen in the "time window" of the fluorescence detection, obviously have no influence on the KCSF signals, as underlined by our pressure dependent data.

At the current stage of the KCSF experiments it is not easy to evaluate the accuracy and uncertainty of this method compared to the KCSI technique. We believe that the results of both methods should be very similar with respect to quality and reliability. In principle, given a detailed set of KCSF curves for several observation windows, excitation wavelengths and bath gases, the results for $P(E',E)$ and the corresponding moments of energy transfer will become "self-calibrated". This means, that the $P(E',E)$ parameters and the shape of the observation windows are automatically determined from the master equation analysis. The results will therefore be independent of any external reference data, as already demonstrated in our KCSI study of azulene.[7]

The fluorescence detection scheme shows considerable potential for studying systems which are not easily accessible for ionization detection. For instance, fluorine substituted aromatics like hexafluorobenzene are very interesting systems because of their much higher collisional efficiency compared to their hydrocarbon analogues.[29–31] However, collisional transition probabilities $P(E',E)$ for these systems have not yet been obtained. Unfortunately, these fluoroaromatics are characterized by high ionization potentials.[32] Possible intermediate electronic states for the KCSI process are located at fairly low energies.[33,34] One-color two-photon ionization is therefore not feasible, and instead a two-color two-photon scheme with two probe lasers would be required. In this case KCSF is clearly the easier approach, and we are currently exploring this avenue. In addition, preliminary results show that KCSF detection can also be successfully applied in very different experimental setups, *e.g.*, within a Laval nozzle expansion to study the collisional deactivation of molecules at ultracold temperatures (>50 K).[35]

References

1 H. Hippler and J. Troe, in *Bimolecular Collisions*, eds. J. E. Baggott and M. N. R. Ashfold, The Royal Society of Chemistry, London, 1989, p. 209.
2 I. Oref and D. C. Tardy, *Chem. Rev.*, 1990, **90**, 1407.
3 M. J. Rossi and J. R. Barker, *Chem. Phys. Lett.*, 1982, **85**, 21.
4 B. M. Toselli, J. D. Brenner, M. L. Yerram, W. E. Chin, K. D. King and J. R. Barker, *J. Chem. Phys.*, 1991, **95**, 176.
5 H. Hippler, J. Troe and H. J. Wendelken, *J. Chem. Phys.*, 1983, **78**, 6709.
6 N. Fay and K. Luther, *Z. Phys. Chem.*, 2000, **214**, 839.
7 U. Hold, T. Lenzer, K. Luther and A. C. Symonds, *J. Chem. Phys.*, 2003, **119**, 11192.
8 U. Hold, T. Lenzer, K. Luther, K. Reihs and A. C. Symonds, *J. Chem. Phys.*, 2000, **112**, 4076.
9 T. Lenzer, K. Luther, K. Reihs and A. C. Symonds, *J. Chem. Phys.*, 2000, **112**, 4090.
10 R. J. Sension, S. T. Repinec and R. M. Hochstrasser, *J. Chem. Phys.*, 1990, **93**, 9185.
11 R. J. Sension, S. T. Repinec, A. Z. Szarka and R. M. Hochstrasser, *J. Chem. Phys.*, 1993, **98**, 6291.
12 L. Nikowa, D. Schwarzer and J. Troe, *Chem. Phys. Lett.*, 1995, **233**, 303.
13 M. Hollerbach, Diploma Thesis, University of Göttingen, Göttingen, 2003.
14 H. Frerichs, M. Hollerbach and T. Lenzer and K. Luther *"Indications for statistical behavior in collisional energy transfer of larger molecules"*, 102nd Bunsentagung, Kiel (Germany), 2003.

15 C. Reichardt, Diploma Thesis, University of Göttingen, Göttingen, 2004.

16 C. S. Burton and W. A. Noyes Jr, *J. Chem. Phys.*, 1968, **49**, 1705.

17 W. Koban, J. D. Koch, R. K. Hanson and C. Schulz, *Phys. Chem. Chem. Phys.*, 2004, **6**, 2940.

18 W. K. Bischel, L. J. Jusinski, M. N. Spencer and D. J. Eckstrom, *J. Opt. Soc. Am. B*, 1985, **2**, 877.

19 J. P. Reilly and K. L. Kompa, *J. Chem. Phys.*, 1980, **73**, 5468.

20 D. S. Zakheim and P. M. Johnson, *Chem. Phys.*, 1980, **46**, 263.

21 J. R. Ackerhalt and J. H. Eberly, *Phys. Rev. A*, 1976, **14**, 1705.

22 C. L. Olson, C. A. Frost, E. L. Patterson and J. W. Poukey, *Trans. Nucl. Sci.*, 1983, **NS–30**, 3189.

23 U. Grigoleit, T. Lenzer, K. Luther, M. Mützel and A. Takahara, *Phys. Chem. Chem. Phys.*, 2001, **3**, 2191.

24 M. Jacon, C. Lardeux, R. Lopez-Delgado and A. Tramer, *Chem. Phys.*, 1977, **24**, 145.

25 M. Klöppel-Riech, PhD Thesis, University of Göttingen, Göttingen, 2000.

26 E. H. Kincaid, V. Worah and M. D. Schuh, *J. Chem. Phys.*, 1991, **94**, 4842.

27 C. G. Hickman, J. R. Gascooke and W. D. Lawrance, *J. Chem. Phys.*, 1996, **104**, 4887.

28 P. Farmanara, V. Stert, W. Radloff and I. V. Hertel, *J. Phys. Chem. A*, 2001, **105**, 5613.

29 M. Damm, H. Hippler, H. A. Olschewski, J. Troe and J. Willner, *Z. Phys. Chem.*, 1990, **166**, 129.

30 T. Lenzer, K. Luther, J. Troe, R. G. Gilbert and K. F. Lim, *J. Chem. Phys.*, 1995, **103**, 626.

31 J. R. Gascooke, Z. T. Alwahabi, K. D. King and W. D. Lawrance, *J. Phys. Chem. A*, 1998, **102**, 8505.

32 C. H. Kwon and M. S. Kim, *J. Chem. Phys.*, 2004, **120**, 11578.

33 D. V. O'Connor, M. Sumitani, J. M. Morris and K. Yoshihara, *Chem. Phys. Lett.*, 1982, **93**, 350.

34 D. Phillips, *J. Chem. Phys.*, 1967, **46**, 4679.

35 B. Abel, B. Hansmann, T. Lenzer and K. Luther, to be published.